THE JOURNAL OF PHYSICAL CHEMISTRY B

Article

Cite This: J. Phys. Chem. B XXXX, XXX, XXX−XXX

pubs.acs.org/JPCB

Cations Modulate Actin Bundle Mechanics, Assembly Dynamics, and Structure

Nicholas Castaneda,[†,‡] Tianyu Zheng,[†,§] Hector J. Rivera-Jacquez,[†] Hyun-Ju Lee,[⊥] Jaekyung Hyun,[⊥] Alexander Balaeff,[†,∥] Qun Huo,[†,§] and Hyeran Kang*[,†,∥]

[†]NanoScience Technology Center, University of Central Florida, Orlando, Florida 32826, United States

[‡]Burnett School of Biomedical Sciences, College of Medicine, University of Central Florida, Orlando, Florida 32827, United States

[§]Department of Chemistry and [∥]Department of Physics, University of Central Florida, Orlando, Florida 32816, United States

[⊥]Electron Microscopy Research Center, Korea Basic Science Institute (KBSI), Cheongju-si, Chungcheongbuk-do 28119, Republic of Korea

Supporting Information

ABSTRACT: Actin bundles are key factors in the mechanical support and dynamic reorganization of the cytoskeleton. High concentrations of multivalent counterions promote bundle formation through electrostatic attraction between actin filaments that are negatively charged polyelectrolytes. In this study, we evaluate how physiologically relevant divalent cations affect the mechanical, dynamic, and structural properties of actin bundles. Using a combination of total internal reflection fluorescence microscopy, transmission electron microscopy, and dynamic light scattering, we demonstrate that divalent cations modulate bundle stiffness, length distribution, and lateral growth. Molecular dynamics simulations of an all-atom model of the actin bundle reveal specific actin residues coordinate cation-binding sites that promote the bundle formation. Our work suggests that specific cation interactions may play a fundamental role in the assembly, structure, and mechanical properties of actin bundles.

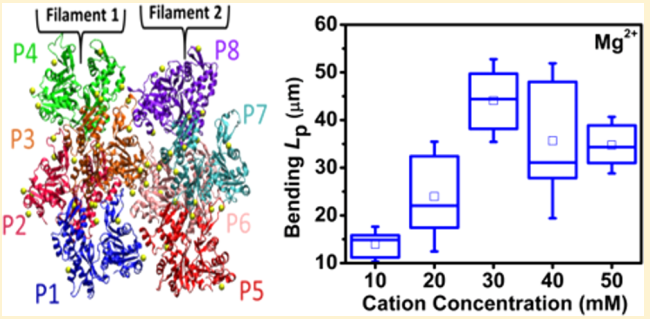

INTRODUCTION

The assembly of actin filaments into ordered bundles provides cells with structural support and mechanical strength for motility.[1−5] Actin filaments are negatively charged linear polyelectrolytes (4 e/nm).[6,7] Multivalent counterions at relatively high concentrations promote actin bundle formation through counterion condensation,[7−13] as described by the polyelectrolyte theory that explains well other polyelectrolytes, such as DNA.[8,9,14] Counterions of higher valence reduce surface charges on actin filaments, leading to charge neutralization.[7] Electrostatic attraction induced by two or more filaments sharing counterions results in structural changes along filaments by overtwisting them within the bundle.[10,15] Filament structure deformation is a potential key factor that determines the mechanical properties of cation-induced actin bundles.

The effects of actin-binding proteins (ABPs) on bundle assembly and mechanics have been well characterized.[1,3,16−18] For example, actin filaments bundled by binding proteins (e.g., fascin, α-actinin, and scruin) have shown to increase bundle stiffness and form tightly packed ordered structures.[1,16,17] Cation effects on mechanics have been demonstrated in other polyelectrolyte systems, such as microtubules[19] and neurofilaments.[20] Although cation effects on actin filament mechanics have been shown,[21] knowledge of how cations modulate the mechanical and dynamic properties of actin bundles is still lacking. It has been proposed that specific cation interactions may contribute to salt-induced bundling of actin filaments.[22] However, molecular mechanisms of how cation binding modulates bundle assembly, structure, and mechanics are not well established.

Here, we investigate how cation interactions modulate the mechanical and dynamic properties of actin bundles using total internal reflection fluorescence (TIRF) microscopy imaging, transmission electron microscopy (TEM), and dynamic light scattering (DLS). We demonstrate that divalent cations modulate the bending stiffness and lateral growth of bundles, whereas cation interactions promote bundling as a dynamic process. Furthermore, we conduct a molecular dynamics (MD) simulation of an all-atom model of the actin bundle to identify specific cation-binding sites on the actin filament. Our MD simulation results demonstrate that cation binding leads to the helical twist of the interacting filaments within the bundle.[10] Taken together, we suggest that the cation interactions provide

Received: January 19, 2018
Revised: February 26, 2018

DOI: 10.1021/acs.jpcb.8b00663
J. Phys. Chem. B XXXX, XXX, XXX−XXX

the basis for actin bundle assembly and have crucial effects on the bundles' mechanical and structural properties.

MATERIALS AND METHODS

Protein and Sample Preparations. Actin was isolated from rabbit skeletal muscle acetone powder, gel filtered over Sephacryl S-300 equilibrated in buffer A (0.2 mM $CaCl_2$, 1 mM NaN_3, 2 mM Tris−HCl pH 8.0, 0.2 mM adenosine 5′-triphosphate (ATP), and 0.5 mM dithiothreitol (DTT)) as described.[21] Rhodamine-labeled rabbit muscle actin (>99% purity) was purchased from Cytoskeleton, Inc. (Denver, CO). Buffer A (50 μL) was added to rhodamine-labeled G-actin to make the concentration 0.4 mg/mL. Calcium-bound G-actin was then subject to cation exchange of Ca^{2+} to Mg^{2+}, 20 mM ethylene glycol-bis(β-aminoethyl ether)-*N*,*N*,*N*′,*N*′-tetraacetic acid (EGTA) and 1 mM $MgCl_2$, equal to the initial concentration of G-actin plus 10 μM was used to convert the calcium-bound G-actin to magnesium bound G-actin.[21] Bundle formation ([actin] = 8 μM, 50% rhodamine-labeled) was induced by the addition of 0.1 volume of 10× polymerization buffers (100 mM imidazole pH 7.0, 10 mM ATP, and 10 mM DTT with varying monovalent (K^+ or Na^+) and divalent (Ca^{2+} or Mg^{2+}) salt concentrations).

Sedimentation Assay. To evaluate bundles at varying cation concentrations, low-speed sedimentation assay[17,18] was performed at 15 000 rpm for 60 min at 4 °C using Sorvall MTX 150 (Thermo Fisher Scientific). After centrifugation, the supernatants were separated and pellets were resuspended with 30 μL of the equivalent polymerization buffer condition. To check for actin in the solutions, a standard sodium dodecyl sodium dodecyl sulfate-polyacrylamide gel electrophoresis (12%) was performed. Wells were labeled as alternating supernatant and pellet conditions to differentiate the samples. The percentage of bundles were quantified using the ImageJ (NIH) gel analysis tools.

TIRF Microscopy Imaging. Actin bundles (50% rhodamine-labeled) were equilibrated for 1 h at room temperature (~22 °C) prior to imaging in varying cation concentrations and were diluted using optical imaging buffer (10−50 mM Ca^{2+} or Mg^{2+}, 1 mM ATP, 1 mM DTT, 10 mM imidazole pH 7.0, 0.15 M glucose, 1 mg/mL catalase, and 0.2 mg/mL glucose oxidase). Cation-induced actin bundles were immobilized on poly-L-lysine (Sigma-Aldrich, St. Louis, MO) coated microscope coverslips. Bundle microscopic images were taken at room temperature (~22 °C) using a Nikon Eclipse Ti TIRF microscope equipped with a Hamamatsu ImagEM X2 CCD camera, a 100× oil immersion objective (numerical aperture 1.49), and Nikon LU-N4 laser. Nikon imaging software Elements (ver. 4.50) was used to image the actin bundles and perform analysis. The size of the pixel in microns was 0.16 μm/pixel determined from the TIRF microscope. Microscope slides were cleaned by absolute ethanol, sonication bath, and then extensive rinsing with ddH_2O as described.[23]

Analysis of Bundle Persistence Length and Length Distribution. Actin bundle persistence length (L_p) and length analysis were performed using ImageJ, *Persistence* software,[24] and OriginLab software as described.[21,23,24] Bending L_p of actin bundles is obtained from the two-dimensional average angular correlation ($\langle C(s)\rangle$) (eq 1) of the tangent angles (θ), which goes along the segment length of the filament (s), A is the scaling factor[21,24,25]

$$\langle C(s)\rangle = \langle \cos[\theta(s) - \theta(0)]\rangle = A\, e^{-x/2L_p} \quad (1)$$

The flexural rigidity of the bundle (k) can be calculated using eq 2, in which L_p is the persistence length and k_BT is the thermal energy.[24]

$$\kappa = L_p k_B T \quad (2)$$

The steady-state length distribution of the actin bundles was fitted using log-normal modeling in eq 3, as described in ref 26.[26,27] y is the probability of the distribution function of bundle lengths, y_0 is the offset value, x_c is the mean center, ω indicates the standard deviation (SD), and A is the area.

$$y = y_0 + \frac{A}{\sqrt{2\pi}\,\omega x}\, e^{(-(\ln(x/x_c))^2/(2\omega^2))} \quad (3)$$

Statistical significance of bundles was determined using OriginLab software by multiple analysis of variance. The probability (p value) between the samples indicated that there is a significant difference between bundles for both divalent cations at various concentrations with a p value of less than 0.05 considered as statistically significant.

TEM Imaging, Bundle Thickness, and Spatial Distribution. Cation-induced bundle (5 μL, [actin] = 10 μM) sample was loaded onto an electron microscopy (EM) grid with continuous carbon film that was rendered hydrophilic by glow discharge. After 60 s sample adsorption, the grid was washed three times using droplets of deionized water, followed by negative staining with 5 μL of 1% uranyl acetate solution. Excess staining solution was blotted using a piece of filter paper. The sample was imaged using a Tecnai G2 Spirit TWIN (FEI Co.) transmission electron microscope operated at 120 kV acceleration voltage. The images were recorded using UltraScan 4000 CCD camera (Gatan Inc.). The diameters of the bundles and interfilament spacing within bundles were quantified using the Nikon Elements (ver. 4.50) software length and intensity tools. The intensity profile showed a series of peaks corresponding to the filaments within the bundle. Distance between the peaks was taken as the distance between the filaments. The number of filaments per each bundle was calculated on the basis of analyzed interfilament spacing, bundle diameter, and known filament diameter (7 nm).[28,29]

Dynamic Light Scattering (DLS). Analyses of all actin bundle sample solutions were performed using a Zetasizer Nano ZS90 DLS system equipped with a green laser (532 nm, 4 mW) and an avalanche photodiode detector (quantum efficiency >50% at 532 nm) (Malvern Instruments Ltd., England). Measured light scattering intensities are displayed as a photon count rate with a unit of kilo count per second (kcps). A Hellma cuvette QS 3 mm was used as sample container. The Malvern DTS 5.10 software was applied to process and analyze the data. The power of incident laser beam was set at 4 mW. For each sample solution, two DLS measurements were performed with a fixed run time of 10 s. The scattering angle was set at 90°. All measurements were conducted at an ambient temperature of 25 °C.

A 50 μL of as-prepared actin monomer solution with the actin concentration of 10 μM was first mixed with 5 μL of 0.1 volume of 10× polymerization buffers separately in a 1.5 mL microcentrifuge tube, followed by quickly transferring into the Hellma cell for measurement. To prevent aggregation of bundles in the cuvette, slight agitation of the solution was performed by minimal disturbance of 10 s before the proceeding time-point. DLS analysis was kinetically conducted every 10 min in a total 2 h time frame. The measurement results were directly reported as photon count rate.

DOI: 10.1021/acs.jpcb.8b00663
J. Phys. Chem. B XXXX, XXX, XXX−XXX

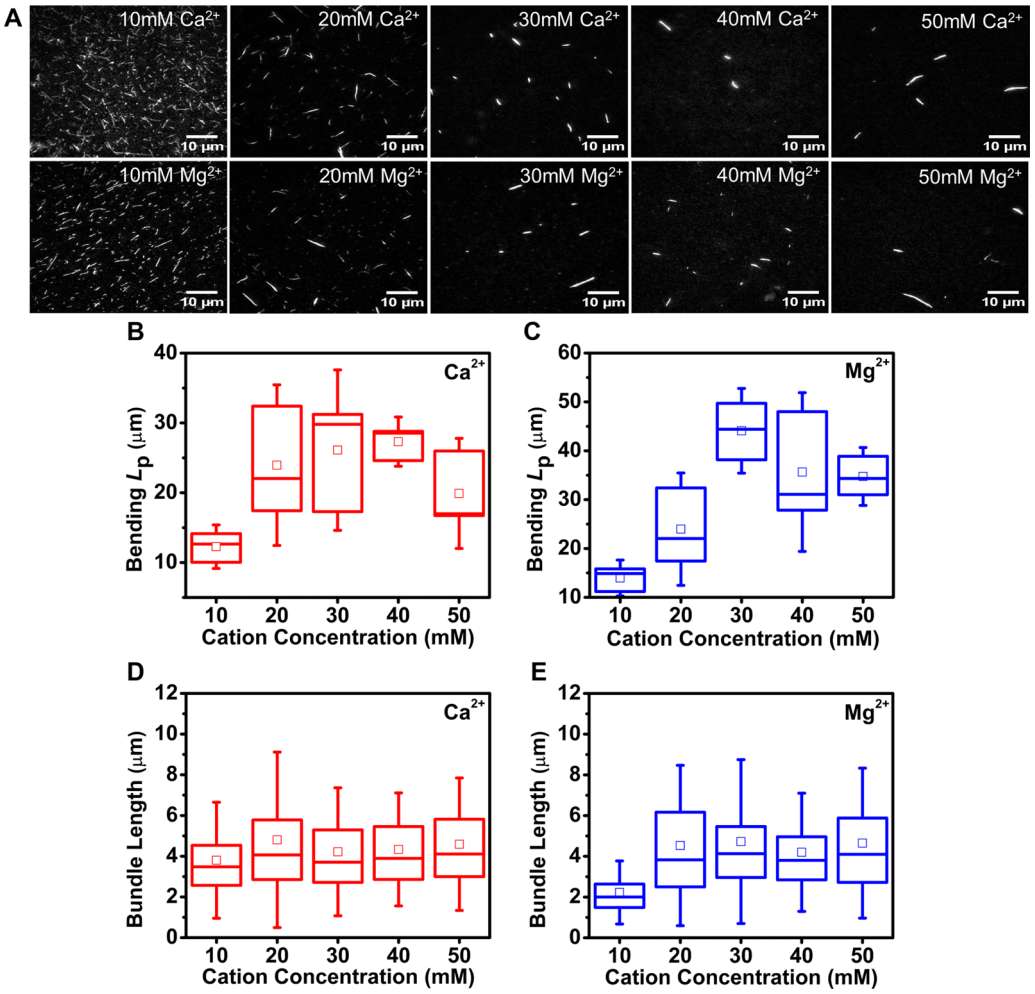

Figure 1. Divalent cations affect the bending stiffness of actin bundles. (A) Representative TIRF microscopy images of actin bundles (8 μM) formed by divalent cations, Ca^{2+} (top) and Mg^{2+} (bottom). Buffers: $CaI_{7.0}$ and $MI_{7.0}$ (10 mM imidazole pH 7.0 with varying [Ca^{2+}] and [Mg^{2+}], 1 mM ATP, and 1 mM DTT; scale bars, 10 μm). (B, C) Bending persistence length (L_p) of actin bundles formed at varying divalent cation concentrations. (D, E) Divalent cation concentration-dependent average bundle length. The box represents the 25th−75th percentile, whiskers indicate standard deviation (SD), and the middle square is the mean. Tukey test indicated significant difference in comparison of L_p values for both Ca^{2+} and Mg^{2+} conditions ($p < 0.05$). Total number of bundles analyzed per each condition $N \approx 250-300$.

Time-Dependent Bundle Fluorescence Analysis. Fluorescence intensity can be a measure of bundle thickness.[30] Imaging of the actin bundles in various time-points was performed using TIRF microscopy. The polymerized bundle samples were placed on microscope coverslips coated with poly-L-lysine (Sigma-Aldrich, St. Louis, MO). The Nikon imaging software allowed for analysis of bundle fluorescence. The diameter was measured by the intensity tool using the Nikon analysis software for each individual bundle sample. Intensity tool was placed along the cross section of each individual bundle. The initial time-point (t = 0 min) was determined by the addition of polymerization buffer into actin sample.

Molecular Dynamics (MD) Simulation. To date, no atomic-resolution experimental structures are available for either the actin filament or the actin bundle. Therefore, our initial all-atom structure of the actin bundle was based on the atomic model of actin filament[29] (PDB ID: 3MFP), called the "Namba model", in the work of Voth and co-authors.[31] The model is based on electron microscopy data and includes two subsequent steps of a two-unit-wide actin filament, i.e., four actin monomers total. Our bundle model was constructed from two Namba tetramers, one of which was translated by 30 Å with respect to the other (Figure 5A). Monomers in the first tetramer are labeled P1−P4, and in the second tetramer, P5−P8.

The thus built all-atom model of the bundle was solvated in a 135 Å × 200 Å × 200 Å box of TIP3P water. Then the system (with the total electrostatic charge of −96 elementary units) was ionized by adding 48 bivalent ions. Two systems were prepared: one with Mg^{2+} and the other with Ca^{2+} ions. The initial placement of the ions was accomplished with MEAD.[32] A 12 Å minimum distance between the ions prevented the ionic clusterization near the potential binding sites. The final structure included 472 695 atoms.

The all-atom simulation of the solvated actin bundle structure was performed with NAMD[33] using CHARMM36 + CMAP force field.[34] The simulations were performed in the NPT regime (the constant temperature of 25 °C and the constant pressure of 1 atm) using periodic boundary conditions, the particle−particle mesh Ewald method[35] for full electrostatic calculations, and a multiple time-stepping scheme with a 2 fs basic time step. The simulation protocol included 25 000 steps of steepest-descent minimization

DOI: 10.1021/acs.jpcb.8b00663
J. Phys. Chem. B XXXX, XXX, XXX−XXX

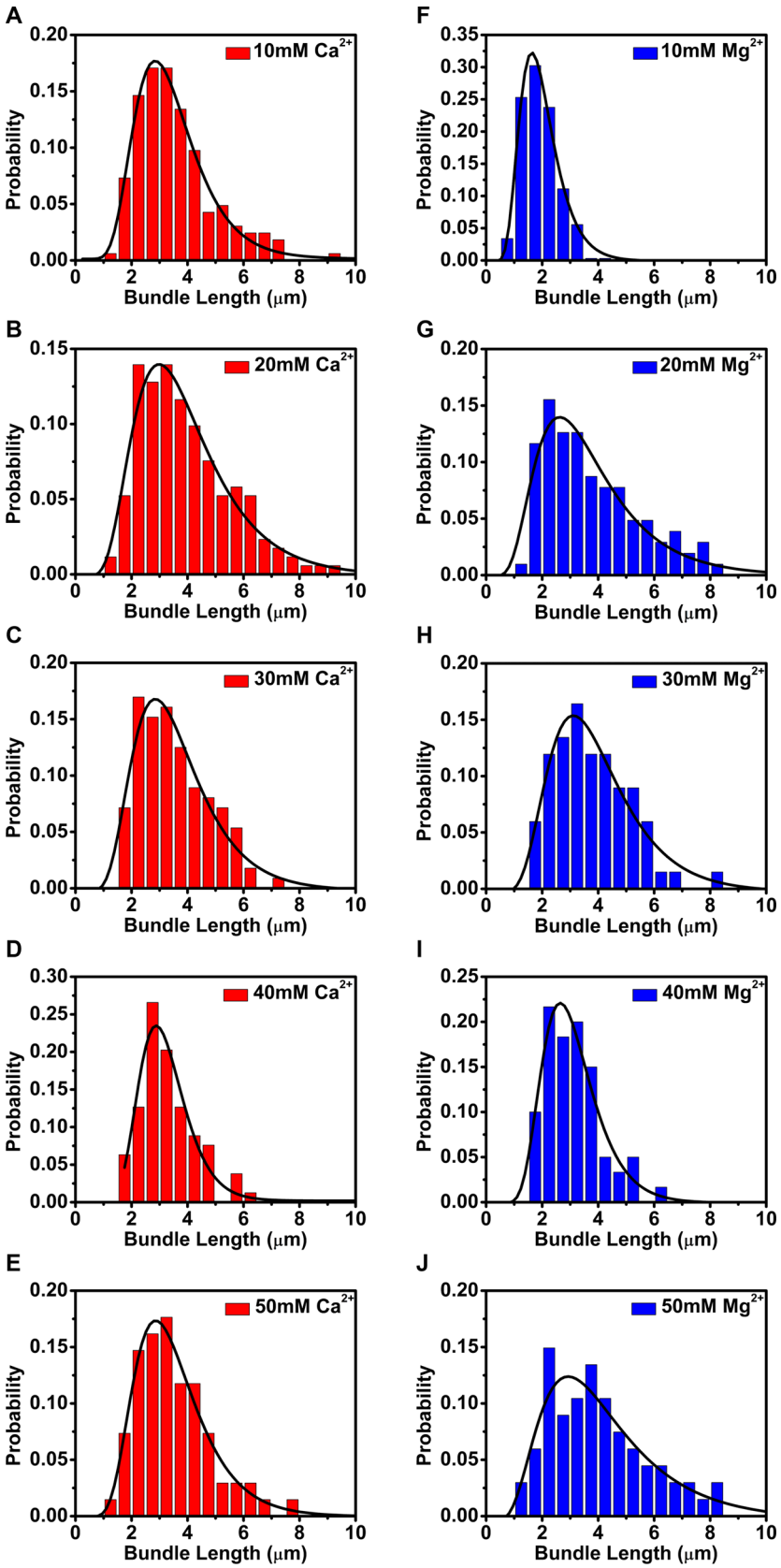

Figure 2. Divalent cations modulate the steady-state length distribution of bundles. The probability distribution of the steady-state bundle length with varying divalent salt concentrations (A–E) Ca^{2+} and (F–J) Mg^{2+} is shown. Solid lines represent the best fits of the data to log-normal distribution model. Polymerization of actin bundles (8 μM) was in buffers: $CaI_{7.0}$ and $MI_{7.0}$ (10 mM imidazole pH 7.0 with varying $[Ca^{2+}]$ and $[Mg^{2+}]$, 1 mM ATP, and 1 mM DTT). Total number of bundles analyzed per each condition $N \approx 250–300$.

DOI: 10.1021/acs.jpcb.8b00663
J. Phys. Chem. B XXXX, XXX, XXX–XXX

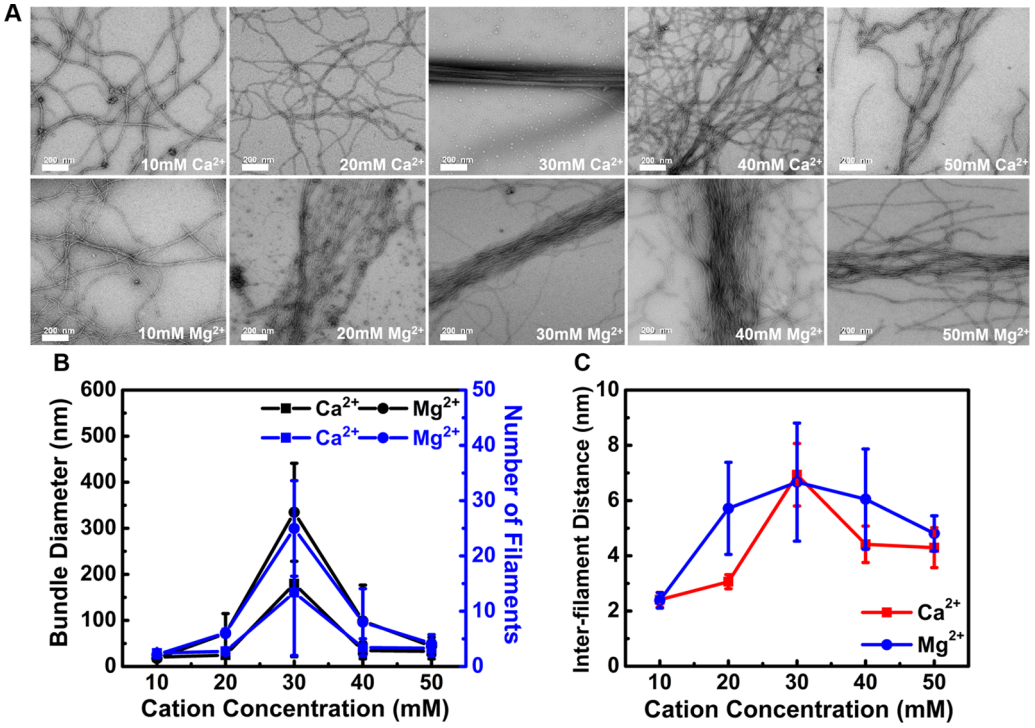

Figure 3. Divalent cations modulate the organization of actin bundles. (A) Representative TEM images of actin bundles ([actin] = 10 μM) demonstrate cation-dependent morphology and organization (scale bars, 200 nm). (B) Bundle diameter and number of filaments per bundle in accordance to varying divalent cation concentrations. (C) Interfilament spacing within bundles is dependent on cation concentration. Polymerization buffers: $CaI_{7.0}$ and $MI_{7.0}$, 10 mM imidazole pH 7.0 with varying [Ca^{2+}] and [Mg^{2+}], 1 mM ATP, and 1 mM DTT. Uncertainty bars represent the SD. Total number of bundles analyzed per each condition $N \approx 20-100$.

followed by a 2 ns equilibration and a 20 ns production run. The coordinates of the atoms of the system were saved every 2 ps, resulting in an MD trajectory of 10 000 frames.

The structural change of the actin bundle during the simulation is described here in terms of the motion of individual actin monomers with respect to their initial positions and orientations of the bundle, namely, the center of mass displacement and the angle of rotation around the center of mass (cf. Figure 5B). The calculation is done for a given monomer at a given time step of the simulation in the following way. First, we perform the best-fit alignment of the whole bundle structure at that time step with the initial structure of the bundle. Next, we perform the best-fit alignment of the given monomer in the aligned bundle with its configuration in the initial bundle. The second alignment is decomposed into the linear vector of the center of mass displacement and the angle and the axis of rotation of the monomer around the center of mass. The distance of displacement and the angle of rotation are the parameters we use to characterize the motion of the individual monomer. The calculations are performed by VMD.[36]

We also characterize the actin bundle structure through the center-of-mass distances between individual monomers (Figure 6). Finally, the ionic binding to the actin bundle is analyzed in terms of ion−filament distances (Figure 5D), defined for each specific cation as the distance to the nearest nonhydrogen atom in a given filament. A bond (permanent or transient) is considered to establish between an ion and a filament if the ion in question is located within 5 Å of the filament.

RESULTS AND DISCUSSION

Divalent Cations Modulate the Mechanical Properties and Length Distribution of Actin Bundles. To determine the flexural rigidity of cation-induced actin bundles, we visualized steady-state bundles formed with physiologically relevant divalent cations (Ca^{2+} or Mg^{2+}) using TIRF microscopy (Figure 1A) and measured the bending L_p from a two-dimensional average cosine correlation analysis[24] (Figure S1). Low-speed sedimentation assay was performed to confirm bundle formation by both divalent cations (Figure S2). Monovalent cations, K^+ or Na^+, do not form actin bundles in the range of concentrations (100−300 mM), consistent with a previous study[37] (Figure S3). The average bending L_p of Ca^{2+}-induced bundles increases by approximately 2-fold, whereas that of Mg^{2+}-induced bundles increases by ∼3-fold over the range of divalent cation concentrations tested (10−50 mM), indicating that both divalent cations stiffen actin bundles (Figure 1B,C).

On average, Mg^{2+}-induced bundles are more rigid than Ca^{2+}-induced bundles, as indicated by the L_p values (Figure 1B,C). Our analysis of L_p suggests bundles stiffen throughout physiological cation concentration of Mg^{2+} (∼18 mM)[38] and with higher concentrations of Ca^{2+}. Although intracellular concentrations of Ca^{2+} are found to be lower (∼100 nM),[39] bundles are still able to form with concentrations similar to those of Mg^{2+}. The difference in the stiffness between Mg^{2+} and Ca^{2+} bundles may be attributed to differences in ionic radius and charge density distribution, which have been shown to affect RNA stability similarly.[40]

The divalent cation-induced bundles are less rigid than those cross-linked by actin-binding proteins (ABPs) (e.g., fascin, α-actinin, or scruin).[1,16,17] Divalent cations stiffen actin bundles

DOI: 10.1021/acs.jpcb.8b00663
J. Phys. Chem. B XXXX, XXX, XXX−XXX

with estimated bending stiffness, $\kappa \sim 0.5-1.7 \times 10^{-25}$ N m^2 for Mg^{2+} and $\kappa \sim 0.5-1.1 \times 10^{-25}$ N m^2 for Ca^{2+}. The mechanical properties of ABP bundles largely depend on cross-linker effectiveness as well as ABP/actin ratios.[1,3,17] Bending stiffness values for bundles cross-linked by binding proteins fascin and α-actinin were similar, with binding protein to actin ratios of 1:2 and 1:10 with ~10 filaments per bundle and $\kappa \sim 1.0 \times 10^{-24}$ N m^2,[1] whereas poly(ethylene glycol) generated bundles indicated $\kappa \sim 1.3 \times 10^{-24}$ N m^2.[1] The cation effects on bundle stiffness could arise from specific cation binding[21] that may work as cross-linker[13] and/or electrostatic screening.[14]

We evaluated how divalent cations affect the steady-state length distribution of actin bundles by analyzing TIRF microscopy images shown in Figure 1A. The average lengths of Ca^{2+}- and Mg^{2+}-induced bundles range from 3.5 to 4.7 μm (Figure 1D,E). Bundle length distribution is fitted to eq 3, and parameters are provided in Table S1. Interestingly, bundle length distance separation is unimodal and falls between 1 and 10 μm, in congruence with a study on Rat2 fibroblast filopodia length distributions.[27] The steady-state length distributions of cation-induced bundles are fit well with log-normal pattern distribution (Figure 2),[27] thereby indicating the logarithm of cation-induced bundle lengths is normally distributed.

Divalent Cations Modulate Actin Bundle Thickness. The effect of cations on bundle thickness is determined by analyzing TEM images that reveal the morphology of actin bundles. Although low cation concentrations (10 mM of Ca^{2+} or Mg^{2+}) induce thin and structurally disorganized bundles, both Ca^{2+} and Mg^{2+} at 30 mM result in the organization of the parallel bundles (Figure 3A), which may indicate a transition from liquid crystalline phase to close-packed assemblies.[10,12] However, at higher concentrations of divalent cations (40 and 50 mM), bundles begin to dissociate from their parallel assemblies (Figure 3A). The dissociation of bundles could be in response to positive bundling energy, being achieved by high divalent cation concentrations.[37] A previous study has demonstrated this phenomena in filamentous virus bundles, so called resolubilization.[41] At low divalent concentrations, filaments show a strong repulsive force, whereas at higher concentrations, filaments are weakly charged with a stronger short-range attraction exceeding repulsive force.[37] In the presence of 30 mM concentrations, the bundles would be large and loosely packed, however, filaments in concentrations that exceed this would present as overcharged with counterions, leading to a reduction in ionic distance, the number of filaments, and interfilament distances (Figure 3B,C).

Both average bundle thickness and the number of filaments per bundle reach a maximum value at 30 mM concentrations (Figure 3B), consistent with a computational study that shows optimal concentration for bundling (~32 mM) at which the bundling energy for two parallel filaments is at its minimum.[37] Ion condensation has been suggested to allow for the charge density between filaments to remain constant and not surpass the packing density,[42] leading to bundle lateral growth. The increase in divalent cation concentrations is observed to broaden bundle diameter distributions (Figure S4).

Distance between filaments within the bundles is determined by further TEM analysis (Figure 3C). Mg^{2+} ions form thicker bundles with higher interfilament spacing than Ca^{2+} ions, which may suggest different attraction energy between filaments induced by two cations.[12] Average interfilament distance of cation-induced bundles ranges from ~2.4 ± 0.3 to 7.0 ± 2.0 nm, indicating that cations form more compact bundles than ABP bundles.[18,43] Reduced spacing between filaments may allow for ions to engage readily with one another across filaments, thereby increasing electrostatic attractions and modulating bundle growth. Actin-binding proteins are limited by their size and protein diameter that can influence filament packing and organization.[18,43,44] Limitations to concentrations and filament spacing for bundling proteins indicate thresholds in assembly,[18,43,44] whereas divalent cations provide the basis for rapid and close-packed bundles without cross-linking proteins.

Divalent Cations Affect Bundle Assembly Dynamics. To determine cation effect on bundle assembly dynamics, we monitored the kinetics of actin bundle formation by utilizing dynamic light scattering (DLS). Low scattering intensity is indicative of actin filaments without an appreciable bundle formation, whereas high scattering intensity is a sign of the filament bundles forming. At 10 μM actin, the DLS intensity follows an upward trend for all salt concentrations, illustrative of bundle formation, with intensity generally being higher for the higher salt concentrations (Figure 4). Occasional intensity peaks indicate transient bundle formation and dissolution at higher salt concentrations (20 and 30 mM Ca^{2+} and Mg^{2+}, respectively), with the maximum peak of 3000 kilo count per second (kcps) observed after 10 min at 20 mM Ca^{2+}.

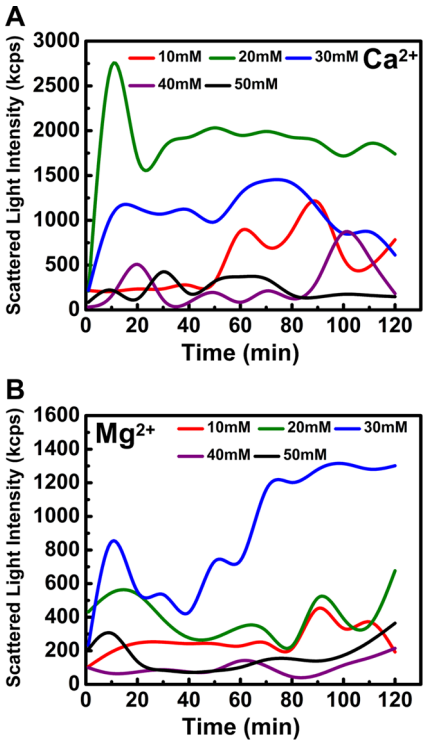

Figure 4. Dynamic light scattering (DLS) indicates kinetic and thermodynamic actin bundle assembly. High variability illustrates dynamic nature of bundling process with (A) Ca^{2+} and (B) Mg^{2+} ([actin] = 10 μM). Scattered light intensity represents bundle formation in kilo count per second (kcps). Experiment performed over 2 h time frame with 10 min interval readings. Measurements were collected at interval readings of 10 s and then averaged (n = 4).

Interestingly, the average DLS intensity profiles correlate well with the time-dependent average bundle lengths and fluorescence intensities measured from TIRF microscopy imaging with varying cation concentrations (Figures S5–S7).

DOI: 10.1021/acs.jpcb.8b00663
J. Phys. Chem. B XXXX, XXX, XXX−XXX

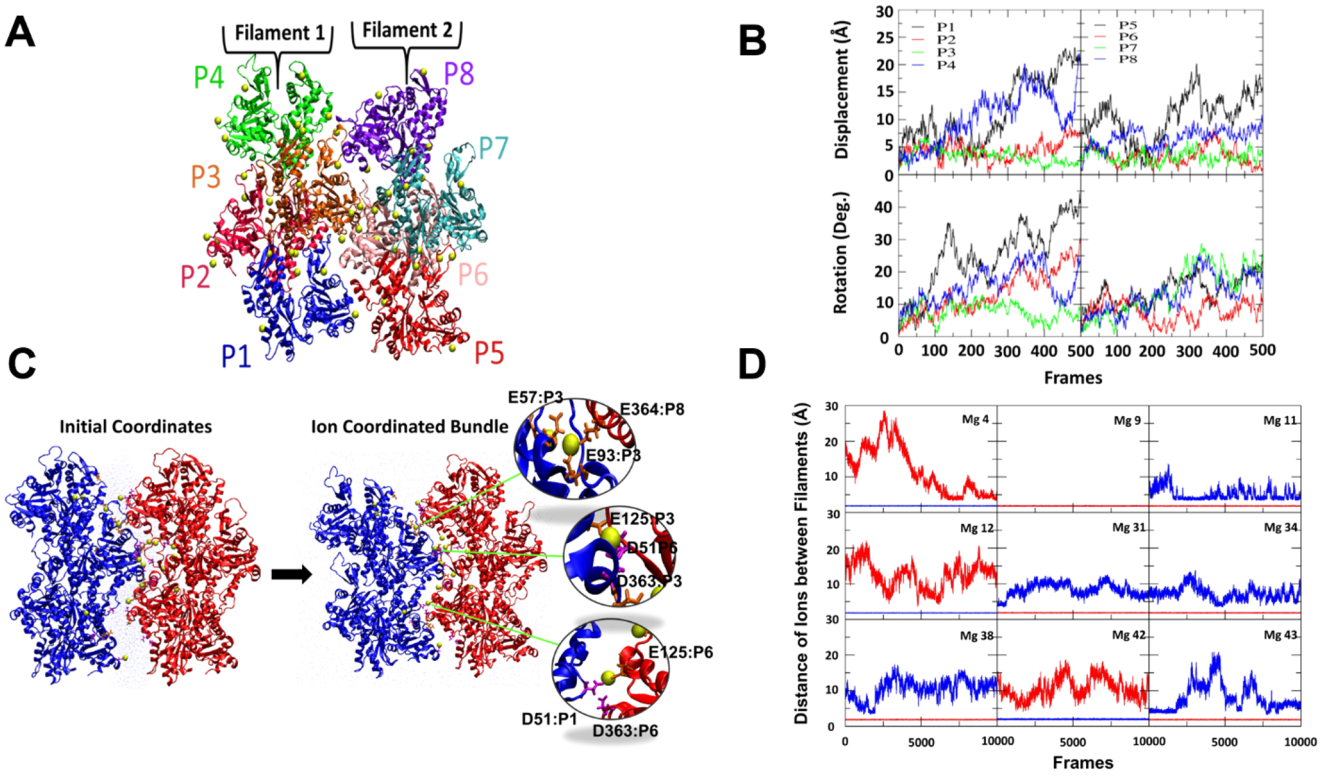

Figure 5. Specific cation interactions promote the structural dynamics of actin bundles. (A) The initial structure of the actin bundle constructed on the basis of the atomic model of actin filament. The longitudinal direction of the bundle is from bottom to top, and the lateral direction is from left to right. Monomers P1−P4 form the first filament, and monomers P5−P8 form the second filament. (B) Displacement and rotation of individual monomers during the simulation with respect to their initial position and orientation. (C) Comparison of the bundle structure before and after the simulation reveals the closing of the solvent gap assisted by the formation of cation-binding sites. Three main cation-binding sites are shown in the insets. (D) The evolution of monomer-ion distances during the MD simulation of the bundle in Mg^{2+} bath (shown for select ions only). Blue lines correspond to the distance from each ion to filament 1 and red lines to filament 2.

Time-dependent average lengths indicate dynamic elongation of bundles (Figure S7A,B), whereas time-dependent fluorescence intensities can serve as an indicator of bundle thickness fluctuations (Figure S7C,D). The fluorescence intensity of bundles correlates with the number of filaments per bundle.[30] However, we note that the number of filaments per bundle (n) estimated from fluorescence intensity (based on TIRF microscopy imaging) could be underestimated compared to direct measurement from TEM images (Figure 3), in particular, for thick bundles ($n > 20$).

There is also a marked behavior of the DLS intensity dynamics on the actin concentration. At 5 μM actin and 20 mM Ca^{2+}/Mg^{2+}, the DLS intensity develops cyclic oscillations with kcps values ranging from 200 to 800 (Figure S8). This behavior suggests a complex interplay of reversible bundle assembly/disassembly dependence on the actin concentration. The bundle formation appears to be favored at early stages of the bundling process. However, over time the disassembly process may catch up with the bundle formation, leading to either a thermodynamically stable state (in terms of the average bundle length and thickness) or an oscillating behavior.

Specific Cation Binding Modulates Actin Bundle Formation and Structure. Recent studies demonstrate that specific cation binding modulates the assembly and mechanical properties of actin filaments.[21,31] We utilize molecular dynamics (MD) simulations to investigate the cation-modulated interactions between the actin filaments within the bundle. To the best of our knowledge, no structure of an actin bundle is available to date. Therefore, we constructed a three-dimensional all-atom structure of an actin bundle based on the well-known Namba model of the filament refined from high-resolution electron cryomicroscopy[29] (PDB ID: 3MFP) (Figure 5A; see Materials and Methods for detailed procedures). Our model bundle includes two actin filaments, four monomers in each. The monomers in filaments 1 and 2 are labeled P1−P4 and P5−P8, respectively (Figure 5A). Most close contacts between the two filaments in the constructed structure are established by the "core" monomers P2−P3 and P6−P7, whereas the "distal" monomers P1/P4 and P5/P8 have fewer contacts with the opposite filament (Figure 5A).

It should be noted that the actin filaments/bundle in the constructed model are four subunits long, whereas one helical period of the actin filament includes 13 subunits.[31] However, the four-monomer bundle length is sufficient for addressing the main topic of this study: the modulating role of cations on the interface between the bundled actin filaments. Expanding the scope of the work toward studying the long-range geometrical parameters of the actin bundle, the bundle rigidity and conformational variance, etc., would require a longer filament model. Yet one cannot build such a model at present, given that the structure of the interface between the actin filaments in the bundle is unknown. This work makes the first step toward understanding the structure of the filament interface.

The constructed model of the actin bundle was subjected to a 20 ns long MD simulation in the bath of water and divalent counterions (see Materials and Method for details). In the

DOI: 10.1021/acs.jpcb.8b00663
J. Phys. Chem. B XXXX, XXX, XXX−XXX

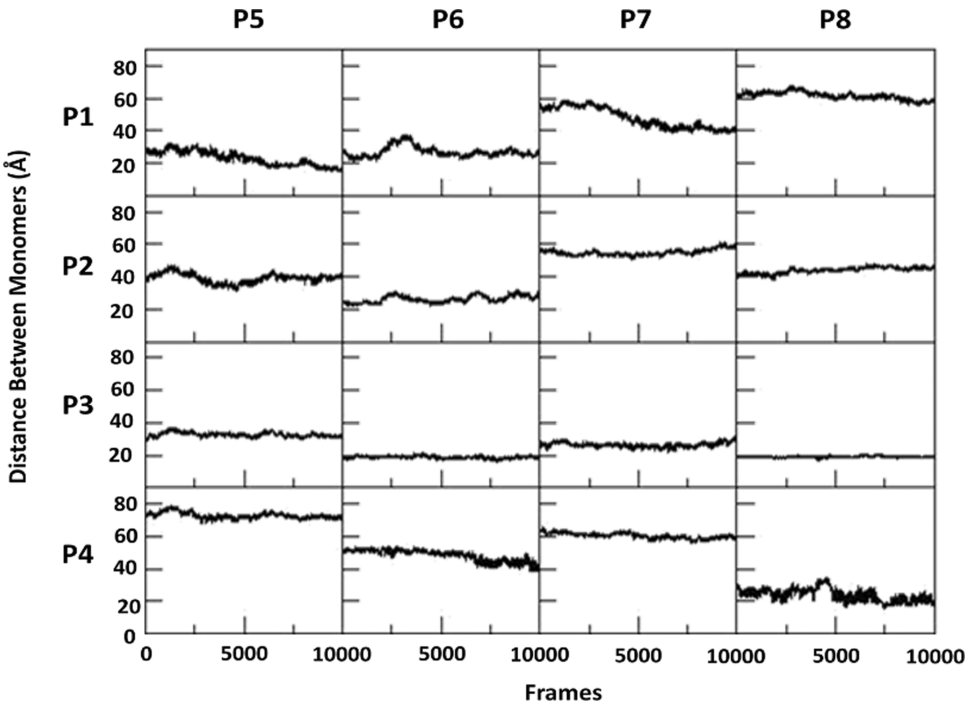

Figure 6. Evolution of the monomer−monomer distance during the molecular dynamics (MD) simulation. Distances between each pair of monomers (labeled P1−P8) within the two filaments in response to cation-induced bundle formation.

course of the simulation, the bundle adapted a more compact structure. The core monomers P2−P3 and P6−P7 oscillated near their initial location/orientation in their respective filaments, whereas the distal monomers P1/P4 and P5/P8 moved and rotated in such a way as to position themselves closer to the neighboring filament (Figures 5B and 6). Furthermore, each of the two filaments in the constructed bundle adapted a helical twist, resulting in the closing of the water channel between the filaments (Figure 5C). This finding is consistent with the previous studies by small-angle X-ray scattering.[10,45]

A further analysis of the simulated actin bundle structure demonstrates the formation of cation bridges that stimulate the two filaments to move close to each other (Figures 5C,D and 6). Most counterions in the simulation are found to be bound to only one filament or none at all, judging by the protein-ionic distances (cf. Materials and Methods). However, three of the ions (Mg4, Mg9, and Mg11: cf. Figure 5C,D) establish close contacts with both filaments by the end of the simulation, i.e., form ionic bridges. The protein sites participating in the bridges are associated with clusters of negatively charged residues on the surface of the protein, especially Asp51, Asp363, and Glu125 (Figure 5C,D). One of the ionic bridges between the core monomers P3−P6 persisted throughout the simulation, whereas the other two bridges drawing the distal monomers P1 and P8 toward the core monomers P6 and P3, respectively, were absent at the beginning of the simulation and formed toward the end when the water channel between the two filaments closed.

CONCLUSIONS

We have investigated the role of cation interactions in mechanical and structural properties of actin bundles using both in vitro experiments and molecular dynamics simulations. We show in this paper that (1) physiologically relevant divalent cations stiffen actin bundles; (2) divalent cations modulate bundle growth and packing; (3) cation-induced bundle formation is a dynamic process that can reach a thermodynamically stable state. Given the results from our MD simulations, it is evident that cation binding at discrete sites on actin filaments leads to bundle formation, resulting in the helical twist of filaments within a bundle. Overall, our results suggest that specific cation binding plays a critical role in actin bundle formation and structure, corroborating the experimental data herein. For future study, it will be interesting to see how site-specific mutations at or near these cation-binding sites affect bundling activities. Such studies will help us understand molecular and cellular mechanisms for cation effects on actin physiology.

ASSOCIATED CONTENT

Supporting Information

The Supporting Information is available free of charge on the ACS Publications website at DOI: 10.1021/acs.jpcb.8b00663.

Average angular correlation functions (Figure S1), low-speed sedimentation (Figure S2), effects of monovalent cations on actin filament assembly (Figure S3), diameter analysis of TEM images (Figure S4), representative TIRF microscopy images of time-dependent Ca^{2+}- and Mg^{2+}-induced bundle assembly (Figures S5 and S6), quantification of cation-induced bundle assembly dynamics (Figure S7), dynamic bundle formation at low actin concentrations (Figure S8); values of log-normal model fitting (Table S1) (PDF)

AUTHOR INFORMATION

Corresponding Author

*E-mail: Hyeran.Kang@ucf.edu.

ORCID

Hector J. Rivera-Jacquez: 0000-0003-3787-5479

DOI: 10.1021/acs.jpcb.8b00663
J. Phys. Chem. B XXXX, XXX, XXX−XXX

Hyeran Kang: 0000-0003-2785-3479

Notes

The authors declare no competing financial interest.

■ ACKNOWLEDGMENTS

This study was supported by the UCF start-up fund (20080739) and In-House grant (63019029) for H.K. TEM analysis was supported by Korea Basic Science Institute grant T37210. This research used resources of the National Energy Research Scientific Computing Center, a DOE Office of Science User Facility supported by the Office of Science of the U.S. Department of Energy under Contract No. DE-AC02-05CH11231. The authors acknowledge the computer time from the UCF STOKES cluster. We thank Dr. Enrique M. De La Cruz for valuable suggestions and critical reading of an earlier version of the manuscript.

■ REFERENCES

(1) Claessens, M. M.; Bathe, M.; Frey, E.; Bausch, A. R. Actin-binding proteins sensitively mediate F-actin bundle stiffness. *Nat. Mater.* **2006**, *5*, 748−753.
(2) Mogilner, A.; Rubinstein, B. The physics of filopodial protrusion. *Biophys. J.* **2005**, *89*, 782−795.
(3) Bathe, M.; Heussinger, C.; Claessens, M. M.; Bausch, A. R.; Frey, E. Cytoskeletal bundle mechanics. *Biophys. J.* **2008**, *94*, 2955−2964.
(4) De La Cruz, E. M.; Gardel, M. L. Actin mechanics and fragmentation. *J. Biol. Chem.* **2015**, *290*, 17137−17144.
(5) Schnauß, J.; Händler, T.; Käs, J. A. Semiflexible biopolymers in bundled arrangements. *Polymers* **2016**, *8*, 274.
(6) Oosawa, F.; Asakura, S. *Thermodynamics of the Polymerization of Protein*; Academic Press, 1975.
(7) Tang, J. X.; Janmey, P. A. The polyelectrolyte nature of F-actin and the mechanism of actin bundle formation. *J. Biol. Chem.* **1996**, *271*, 8556−8563.
(8) Manning, G. S. Limiting laws and counterion condensation in polyelectrolyte solutions. V. Further development of the chemical model. *Biophys. Chem.* **1978**, *9*, 65−70.
(9) Manning, G. S. The molecular theory of polyelectrolyte solutions with applications to the electrostatic properties of polynucleotides. *Q. Rev. Biophys.* **1978**, *11*, 179−246.
(10) Angelini, T. E.; Liang, H.; Wriggers, W.; Wong, G. C. Like-charge attraction between polyelectrolytes induced by counterion charge density waves. *Proc. Natl. Acad. Sci. U.S.A.* **2003**, *100*, 8634−8637.
(11) Manning, G. S. Counterion condensation on charged spheres, cylinders, and planes. *J. Phys. Chem. B* **2007**, *111*, 8554−8559.
(12) Wong, G. C.; Pollack, L. Electrostatics of strongly charged biological polymers: Ion-mediated interactions and self-organization in nucleic acids and proteins. *Annu. Rev. Phys. Chem.* **2010**, *61*, 171−189.
(13) Janmey, P. A.; Slochower, D. R.; Wang, Y. H.; Wen, Q.; Cebers, A. Polyelectrolyte properties of filamentous biopolymers and their consequences in biological fluids. *Soft Matter* **2014**, *10*, 1439−1449.
(14) Manning, G. S. Counterion binding in polyelectrolyte theory. *Acc. Chem. Res.* **1979**, *12*, 443−449.
(15) Angelini, T. E.; Sanders, L. K.; Liang, H.; Wriggers, W.; Tang, J. X.; Wong, G. C. Structure and dynamics of condensed multivalent ions within polyelectrolyte bundles: a combined X-ray diffraction and solid-state NMR study. *J. Phys.: Condens. Matter* **2005**, *17*, S1123−S1135.
(16) Shin, J. H.; Mahadevan, L.; So, P. T.; Matsudaira, P. Bending stiffness of a crystalline actin bundle. *J. Mol. Biol.* **2004**, *337*, 255−261.
(17) Takatsuki, H.; Bengtsson, E.; Mansson, A. Persistence length of fascin-cross-linked actin filament bundles in solution and the in vitro motility assay. *Biochim. Biophys. Acta* **2014**, *1840*, 1933−1942.
(18) Jansen, S.; Collins, A.; Yang, C.; Rebowski, G.; Svitkina, T.; Dominguez, R. Mechanism of actin filament bundling by fascin. *J. Biol. Chem.* **2011**, *286*, 30087−30096.
(19) Needleman, D. J.; Ojeda-Lopez, M. A.; Raviv, U.; Miller, H. P.; Wilson, L.; Safinya, C. R. Higher-order assembly of microtubules by counterions: from hexagonal bundles to living necklaces. *Proc. Natl. Acad. Sci. U.S.A.* **2004**, *101*, 16099−16103.
(20) Beck, R.; Deek, J.; Choi, M. C.; Ikawa, T.; Watanabe, O.; Frey, E.; Pincus, P.; Safinya, C. R. Unconventional salt trend from soft to stiff in single neurofilament biopolymers. *Langmuir* **2010**, *26*, 18595−18599.
(21) Kang, H.; Bradley, M. J.; McCullough, B. R.; Pierre, A.; Grintsevich, E. E.; Reisler, E.; De La Cruz, E. M. Identification of cation-binding sites on actin that drive polymerization and modulate bending stiffness. *Proc. Natl. Acad. Sci. U.S.A.* **2012**, *109*, 16923−16927.
(22) Kang, H.; Bradley, M. J.; Elam, W. A.; De La Cruz, E. M. Regulation of actin by ion-linked equilibria. *Biophys. J.* **2013**, *105*, 2621−2628.
(23) Kang, H.; Bradley, M. J.; Cao, W.; Zhou, K.; Grintsevich, E. E.; Michelot, A.; Sindelar, C. V.; Hochstrasser, M.; De La Cruz, E. M. Site-specific cation release drives actin filament severing by vertebrate cofilin. *Proc. Natl. Acad. Sci. U.S.A.* **2014**, *111*, 17821−17826.
(24) Graham, J. S.; McCullough, B. R.; Kang, H.; Elam, W. A.; Cao, W.; De La Cruz, E. M. Multi-platform compatible software for analysis of polymer bending mechanics. *PLoS One* **2014**, *9*, No. e94766.
(25) McCullough, B. R.; Grintsevich, E. E.; Chen, C. K.; Kang, H.; Hutchison, A. L.; Henn, A.; Cao, W.; Suarez, C.; Martiel, J. L.; Blanchoin, L.; et al. Cofilin-linked changes in actin filament flexibility promote severing. *Biophys. J.* **2011**, *101*, 151−159.
(26) Limpert, E.; Stahel, W. A.; Abbt, M. Log-normal Distributions across the Sciences: Keys and Clue. *BioScience* **2001**, *51*, 341−352.
(27) Husainy, A. N.; Morrow, A. A.; Perkins, T. J.; Lee, J. M. Robust patterns in the stochastic organization of filopodia. *BMC Cell Biol.* **2010**, *11*, 86.
(28) Blanchoin, L.; Boujemaa-Paterski, R.; Sykes, C.; Plastino, J. Actin dynamics, architecture, and mechanics in cell motility. *Physiol. Rev.* **2014**, *94*, 235−263.
(29) Fujii, T.; Iwane, A. H.; Yanagida, T.; Namba, K. Direct visualization of secondary structures of F-actin by electron cryomicroscopy. *Nature* **2010**, *467*, 724−728.
(30) Breitsprecher, D.; Koestler, S. A.; Chizhov, I.; Nemethova, M.; Mueller, J.; Goode, B. L.; Small, J. V.; Rottner, K.; Faix, J. Cofilin cooperates with fascin to disassemble filopodial actin filaments. *J. Cell Sci.* **2011**, *124*, 3305−3318.
(31) Hocky, G. M.; Baker, J. L.; Bradley, M. J.; Sinitskiy, A. V.; De La Cruz, E. M.; Voth, G. A. Cations stiffen actin filaments by adhering a key structural element to adjacent subunits. *J. Phys. Chem. B* **2016**, *120*, 4558−4567.
(32) Bashford, D. An object-oriented programming suite for electrostatic effects in biological molecules an experience report on the MEAD project. *Lect. Notes Comput. Sci.* **1997**, *1343*, 233−240.
(33) Phillips, J. C.; Braun, R.; Wang, W.; Gumbart, J.; Tajkhorshid, E.; Villa, E.; Chipot, C.; Skeel, R. D.; Kale, L.; Schulten, K. Scalable molecular dynamics with NAMD. *J. Comput. Chem.* **2005**, *26*, 1781−1802.
(34) Best, R. B.; Zhu, X.; Shim, J.; Lopes, P. E.; Mittal, J.; Feig, M.; MacKerell, A. D., Jr. Optimization of the additive CHARMM all-atom protein force field targeting improved sampling of the backbone ϕ, ψ and side-chain χ1 and χ2 dihedral angles. *J. Chem. Theory Comput.* **2012**, *8*, 3257−3273.
(35) Darden, T.; York, D.; Pedersen, L. Particle mesh Ewald: An N·log (N) method for Ewald sums in large systems. *J. Chem. Phys.* **1993**, *98*, 10089−10092.
(36) Humphrey, W.; Dalke, A.; Schulten, K. VMD: visual molecular dynamics. *J. Mol. Graphics* **1996**, *14*, 33−38.
(37) Yu, X.; Carlsson, A. E. Multiscale study of counterion-induced attraction and bundle formation of F-actin using an Ising-like mean-field model. *Biophys. J.* **2003**, *85*, 3532−3543.
(38) Romani, A. M. Cellular magnesium homeostasis. *Arch. Biochem. Biophys.* **2011**, *512*, 1−23.

DOI: 10.1021/acs.jpcb.8b00663
J. Phys. Chem. B XXXX, XXX, XXX−XXX

(39) Forsen, S.; Kordel, J. *Calcium in Biological Systems*; University Science Books: Mill Valley, CA, 1994; p 107.
(40) Koculi, E.; Hyeon, C.; Thirumalai, D.; Woodson, S. A. Charge density of divalent metal cations determines RNA stability. *J. Am. Chem. Soc.* **2007**, *129*, 2676−2682.
(41) Tang, J. X.; Janmey, P. A.; Lyubartsev, A.; Nordenskiold, L. Metal ion-induced lateral aggregation of filamentous viruses fd and M13. *Biophys. J.* **2002**, *83*, 566−581.
(42) Henle, M. L.; Pincus, P. A. Equilibrium bundle size of rodlike polyelectrolytes with counterion-induced attractive interactions. *Phys. Rev. E* **2005**, *71*, No. 060801.
(43) Winkelman, J. D.; Suarez, C.; Hocky, G. M.; Harker, A. J.; Morganthaler, A. N.; Christensen, J. R.; Voth, G. A.; Bartles, J. R.; Kovar, D. R. Fascin-and α-actinin-bundled networks contain intrinsic structural features that drive protein sorting. *Curr. Biol.* **2016**, *26*, 2697−2706.
(44) Bartles, J. R. Parallel actin bundles and their multiple actin-bundling proteins. *Curr. Opin. Cell. Biol.* **2000**, *12*, 72−78.
(45) Claessens, M. M.; Semmrich, C.; Ramos, L.; Bausch, A. R. Helical twist controls the thickness of F-actin bundles. *Proc. Natl. Acad. Sci. U.S.A.* **2008**, *105*, 8819−8822.

DOI: 10.1021/acs.jpcb.8b00663
J. Phys. Chem. B XXXX, XXX, XXX−XXX